

Studying the WHIM Content of the Galaxy Large-Scale Structures along the Line of Sight to H 2356-309

L. Zappacosta^{1,2}, F. Nicastro^{1,3,4}, R. Maiolino³, G. Tagliaferri⁵, D.A. Buote⁶, T. Fang⁶, P.J. Humphrey⁶, F. Gastaldello⁷

Harvard-Smithsonian Center for Astrophysics, Cambridge, MA, 02138, USA

ABSTRACT

We make use of a 500 ks Chandra HRC-S/LETG spectrum of the blazar H 2356-309, combined with a lower S/N (100 ks) pilot LETG spectrum of the same target, to search for the presence of warm-hot absorbing gas associated with two Large-Scale Structures (LSSs) crossed by this sightline, and to constrain its physical state and geometry. Strong ($\log N_{\text{OVII}} \geq 10^{16} \text{ cm}^{-2}$) OVII $K\alpha$ absorption associated with a third LSS crossed by this line of sight (the Sculptor Wall, SW), at $z = 0.03$, has already been detected in a previous work. Here we focus on two additional prominent filamentary LSSs along the same line of sight, at $z=0.062$ (the Pisces-Cetus Supercluster, PCS) and at $z=0.128$ (the “Farther Sculptor Wall”, FSW).

The combined LETG spectrum has a S/N of $\sim 11.6 - 12.6$ per resolution element in the $20 - 25 \text{ \AA}$, and an average 3σ sensitivity to intervening OVII $K\alpha$ absorption line equivalent widths of $\text{EW}_{\text{OVII}} \gtrsim 14 \text{ m\AA}$ in the available redshift range ($z < 0.165$). No statistically significant (i.e. $\geq 3\sigma$) individual absorption is detected from any of the strong He- or H-like transitions of C, O and Ne (the most abundant metals in gas with solar-like composition) at the redshifts of the

¹Harvard-Smithsonian Center for Astrophysics, 60 Garden Street, Cambridge, MA 02138; lzappacosta@cfa.harvard.edu

²INAF - Osservatorio Astronomico di Trieste, via G.B. Tiepolo 11, I-34143, Trieste, Italy.

³INAF - Osservatorio Astronomico di Roma, via di Frascati 33, 00040 Monte Porzio Catone, Italy

⁴IESL, Foundation for Research and Technology, 71110, Heraklion, Crete (Greece)

⁵INAF - Osservatorio Astronomico di Brera, via Bianchi 46, 23807 Merate (LC), Italy

⁶Department of Physics and Astronomy, 4129 Frederick Reines Hall, University of California, Irvine, CA 92697

⁷INAF - IASF, via Bassanini 15, I-20133 Milano, Italy; Occhialini Fellow

PCS and FSW structures, and down to the above EW thresholds. However we are still able to constrain the physical and geometrical parameters of the putative absorbing gas associated with these structures, by performing joint spectral fit of various marginal detections and upper limits of the strongest expected lines with our self-consistent hybrid ionization WHIM spectral model.

At the redshift of the PCS we identify a warm phase with $\log T = 5.35_{-0.13}^{+0.07}$ K and $\log N_{\text{H}} = (19.1 \pm 0.2)$ cm^{-2} possibly coexisting with a much hotter and statistically less significant phase with $\log T = 6.9_{-0.8}^{+0.1}$ K and $\log N_{\text{H}} = 20.1_{-1.7}^{+0.3}$ cm^{-2} (1σ errors). These two separate physical phases are identified through, and mainly constrained by, CV $\text{K}\alpha$ (warm phase) and OVIII $\text{K}\alpha$ (hot phase) absorption, with single line significances of 1.5σ each.

For the second LSS, at $z \simeq 0.128$, only one hot component is hinted in the data, through OVIII $\text{K}\alpha$ (1.6σ) and NeIX $\text{K}\alpha$ (1.2σ). For this system, we estimate $\log T = 6.6_{-0.2}^{+0.1}$ K and $\log N_{\text{H}} = 19.8_{-0.8}^{+0.4}$ cm^{-2} .

Our column density and temperature constraints on the warm-hot gaseous content of these two LSSs, combined with the measurements obtained for the hot gas permeating the SW, allow us to estimate the cumulative number density per unit redshifts of OVII WHIM absorbers at 3 different equivalent width thresholds of $0.4\text{m}\text{\AA}$, $7\text{m}\text{\AA}$ and $25.8\text{m}\text{\AA}$. This is consistent with expectations only at the very low end of EW thresholds, but exceed predictions at $7\text{m}\text{\AA}$ and $25.8\text{m}\text{\AA}$ (by more than 2σ). We also estimate the cosmological mass density of the WHIM based on the 4 absorbers we tentatively detect along this line of sight, obtaining $\Omega_b^{\text{WHIM}} = (0.021_{-0.018}^{+0.031})(Z/Z_{\odot})^{-1}$, consistent with the cosmological mass density of the intergalactic ‘missing baryons’ only if we assume high metallicities ($Z \sim Z_{\odot}$).

Subject headings: intergalactic medium, large-scale structure of universe

1. Introduction

Cosmological hydrodynamical simulations predict the gradual formation of a local ($z < 1$) web of low density ($n_b = 10^{-6} - 10^{-5} \text{cm}^{-3}$), warm-hot ($T = 10^5 - 10^7$ K) intergalactic gas, connecting virialized halos (i.e. galaxies, galaxy groups and clusters of galaxies), permeating the large-scale structures (LSS) of which these systems are constituents, and ultimately providing the necessary fuel for their continuous growth (Cen et al. 1995; Cen & Ostriker 1999; Davé et al. 2001; Cen & Ostriker 2006). This low-redshift intergalactic gas is largely the same primordial gas present at redshift higher than ~ 2 in a cool photo-ionized phase

(the so called 'Lyman- α Forest)', but in a much hotter and metal-enriched phase, because of efficient shock-heating during the continuous process of LSS assembly and growth in a non-linear Universe, and of strong feedback with the same structures for which it provides building blocks. Due to its high temperatures this IGM phase has been dubbed Warm-Hot Intergalactic Medium (WHIM).

Electrons and baryons in the WHIM are shock-heated during their infall in the dark matter LSS potential well, and settle in filamentary/sheet-like structures surrounding LSSs. Such matter is predicted to account for a sizable fraction ($\sim 50\%$) of all the baryons in the local ($z < 1$) universe, and it is thus considered the best candidate to host the baryons seen at high redshift and missing from the low redshift census (Fukugita et al. 1998; Fukugita & Peebles 2004).

Given its high temperature the WHIM can only emit or absorb in the Far UV and soft X-rays, mainly through Li- through H-like metal transitions and bremsstrahlung continuum emission. However, at WHIM densities both line and continuum emission are highly depressed (due to the dependency of these mechanisms on the square power of the emitters volume densities), and on average well below the sensitivity of current instrumentations. Nonetheless, statistical techniques based on cross correlation of regions with excess diffuse X-ray emission in ROSAT, *Chandra* and XMM-*Newton* deep exposures, with large-scale galaxy distribution, have probably already allowed the marginal detection of the density peak of the WHIM distribution (e.g. Scharf et al. 2000; Zappacosta et al. 2002, 2005; Werner et al. 2008).

A far more promising way to detect the WHIM is through resonant absorption by highly ionized metals. Intervening WHIM filaments should imprint a 'forest', i.e. the so called X-ray Forest (Hellsten et al. 1998; Perna & Loeb 1998), by analogy with the HI Ly α Forest copiously seen at $z \gtrsim 2$, of metal absorption lines onto the spectra of bright background sources, whose strength depends only linearly on the absorber density, and is therefore less suppressed than the corresponding emission. Predicted equivalent widths (EWs) from the most abundant ions in WHIM, range from 1 mÅ to $\lesssim 20$ mÅ for the densest filaments. The detection of even the strongest of such absorption lines (probing only the very high density tail of the WHIM distribution: overdensity $\delta = n_b / \langle n_b \rangle \gtrsim 300$, compared to the average density of the Universe: $\langle n_b \rangle = 2 \times 10^{-7} (1+z)^3 (\Omega_b h^2 / 0.02)$, where Ω_b is the baryonic density parameter and h is the Hubble constant in units of 100 km/s/Mpc) is extremely challenging with the limited sensitivity ($A_{eff} < 60 \text{ cm}^2$) and resolution ($R = E / \Delta E = 400 - 800$) of the current *Chandra* and XMM-*Newton* high resolution X-ray gratings. A $\geq 3\sigma$ detection of an EW=20 mÅ absorption line, requires spectra of the background targets with $S/N \gtrsim 8$ per 50 mÅ resolution element (i.e. $\gtrsim 70$ net counts per bin). These can only be

obtained, for the brightest ($\sim 10^{-11} \text{erg s}^{-1} \text{cm}^{-2}$) soft X-ray (0.5 – 2 keV) targets in the extragalactic sky (preferably blazars, because of their intrinsically featureless spectra), with $\gtrsim 0.5$ Ms exposures, while in quiescence, or $\gtrsim 100$ ks exposures in outburst.

Such dense WHIM filaments are rare. According to hydrodynamical simulations, at $z \simeq 0$ one expects ≤ 0.05 WHIM filaments with $\text{EW}(\text{OVII}_{K\alpha}) \geq 20 \text{ m}\text{\AA}$, per unit redshift. The probability of having one of such filaments along a random line of sight up to $z = 0.3$, is therefore only 1.5% (Gehrels 1986), and only few $z \geq 0.3$ targets with quiescent $\text{F}(0.5\text{--}2 \text{ keV}) \geq 10^{-11} \text{ erg s}^{-1} \text{ cm}^{-2}$ are available (e.g. Conciatore et al., 2009, priv. comm.). The number density of OVII WHIM absorbers per unit redshift increases by almost two orders of magnitude by lowering the $\text{EW}(\text{OVII}_{K\alpha})$ detection threshold down to $\geq 2 \text{ m}\text{\AA}$ so dramatically increasing the probability of randomly detecting one of such filaments to $\text{P}(z = 0.3) = 97.5\%$. This observational strategy has the advantage to probe, in theory, the bulk of the WHIM mass distribution, but requires incredibly high S/N spectra (≥ 75 per resolution element with the *Chandra* LETG, and ≥ 180 per resolution element with the *XMM-Newton* RGS, for a $\geq 3\sigma$ detection), obtainable only with several Ms exposures on the brightest possible $z \geq 0.3$ targets in their quiescent states. Moreover, even when such high S/N spectra are obtained (for example by observing background target during exceptionally high outburst: Nicastro et al. 2005a,b) the clear assessment of the statistical significance of such weak 2-3 mÅ absorption lines is hampered by our limited knowledge of the instrument systematics, which is comparable to the statistical uncertainties on the lines EWs (Kaastra et al. 2003; Rasmussen et al. 2007; Nicastro et al. 2008)

An alternative observational strategy is to select lines of sight where the probability to cross dense WHIM filament is enhanced (e.g. Zappacosta 2005, 2006). WHIM gas density and metallicity is predicted (and possibly in the UV observed Stocke et al. 2006) to correlate with LSS galaxy overdensity (Viel et al. 2005). Thus, chances of intercepting a dense WHIM filament may be improved by carefully selecting bright sources in the background of extreme filamentary LSS concentrations (Fig. 1). This observational strategy has been successfully exploited recently in Buote et al. (2009), who detected a strong ($\text{EW} \sim 30 \text{ m}\text{\AA}$) absorption line in two *XMM-Newton* RGS and *Chandra* LETG spectra of the blazar H 2356-309 ($z=0.165$), and tentatively identified it with OVII $K\alpha$ at a redshift consistent with that spanned by the intervening Sculptor Wall (SW; da Costa et al. 1988).

Here, and in our companion paper (Fang et al. 2009), we report on the successful extension of this observational program. H 2356-309 has been recently re-observed with the *Chandra* LETG for 500 ks, as part of an approved cycle 10 GO observational program. The main goal of this deep observation was to confirm, at higher significance, the SW OVII detection (Fang et al. 2009). Secondary objectives, were to confirm the presence of other (lower

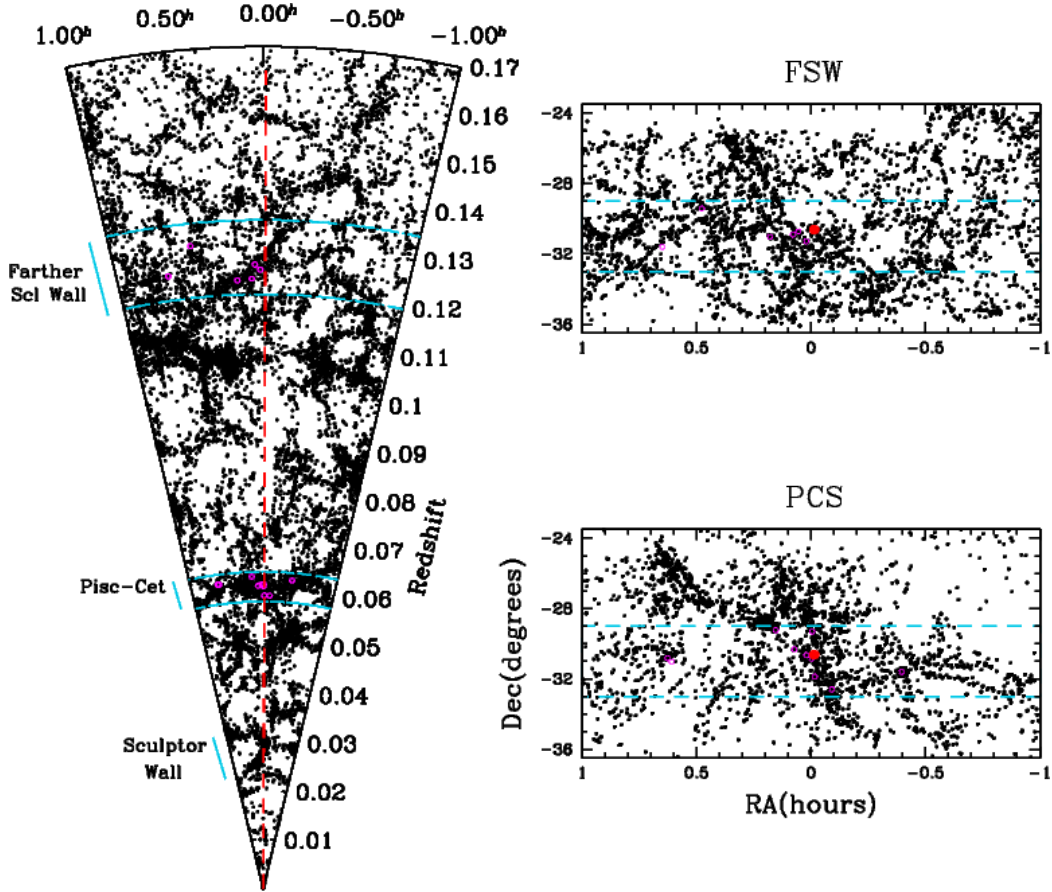


Fig. 1.— Sky map and wedge diagram of the region of the Sculptor Wall where the blazar H 2356-309 is located. The upper sky map refer to the FSW and the lower to the PCS. Galaxies (black point) clusters and groups of galaxies (magenta circles) in the wall are taken from NED. The wedge diagram show galaxies inside the dashed blue box drawn in the sky map and report the sightline to the blazar as red dashed line. The galaxy and cluster catalogs contain objects belonging to different parent catalogs. Hence we point out that some holes in the projected galaxy distribution are artificially caused by this non homogeneity like the hole at north-east of the blazar position visible at RA = 0.1hours and DEC = -29.5deg in the PCS sky map.

significance) lines from the same absorber (Buote et al., 2010 in prep.). Here instead we focus on constraining the physical parameters of the putative WHIM gas content of two additional galaxy LSSs present along this line of sight, at $z = 0.062$ (the Pisces-Cetus Supercluster; PCS) and $z = 0.128$ (a farther wall which we will call Farther Sculptor Wall; FSW). In this paper we use all the existing *Chandra* LETG data of H 2356-309, to characterize the physical properties of the WHIM permeating these additional structures, and conclude by estimating the contribution of such dense gaseous component of LSSs, to the WHIM cosmological mass density. In §2 we describe the richness of LSSs along the line of sight to H 2356-309. In §3 and §4 we present the data and describe their reduction and analysis. §5 is devoted to a critical discussion of our findings. In §6 we summarize our conclusions. Throughout the paper we adopt a Λ -CDM cosmology, with $h = 0.71$, $\Omega_M = 0.27$, $\Omega_\Lambda = 0.73$.

2. The LSS Richness of the Line of Sight to H 2356-309

Figure 1 shows the wedge diagram of the line of sight to H 2356-309 in the declination range $-33 < \delta < -29$. Galaxies (black point), clusters and groups of galaxies (magenta circles) shown in the diagrams of Fig. 1, are extracted from a number of different and non-homogeneous catalogs and galaxy surveys (including the 2dF Galaxy Redshift Survey - 2dFGRS, Colless et al. 2003; and 6dF Galaxy Redshift Survey - 6dFGRS, Jones et al. 2004), and are the result of a general query to the Nasa/Ipac Extragalactic Database (NED)¹. As such, these diagrams do not represent complete flux-limited sample of the actual galaxy distribution along this line of sight.

Several strong LSS concentrations are clearly visible, and cross the line of sight to H 2356-309 at, at least, three different average redshifts: $\langle z_1 \rangle = 0.03$ (the SW), $\langle z_2 \rangle = 0.062$ (the PCS), and $\langle z_3 \rangle = 0.128$ (the FSW). Both the PCS and the FSW LSSs are significantly larger than the SW, and are delimited in the wedge diagram of Fig. 1 by cyan dashed arcs. The two 2D sky map projections on the right of the wedge diagram of Fig. 1, show the RA versus DEC extent of these two LSSs.

The PCS (Burns & Batuski 1984; Tully et al. 1992) is one of the richest nearby ($z < 0.1$) superclusters. It is clearly visible in the SDSS and 2dF redshift surveys as a remarkable filament of galaxies (Porter & Raychaudhury 2005). The structure intercepted by the line of sight to H 2356-309 is a long filament of galaxies located on the plane of the sky at $z=0.06-0.063$, within $< 1Mpc$ from the projected blazar position.

¹The NASA/IPAC Extragalactic Database (NED) is operated by the Jet Propulsion Laboratory, California Institute of Technology, under contract with the National Aeronautics and Space Administration.

The FSW is a conspicuous wall of galaxies, which originates from the Sculptor Supercluster at $z=0.11$, and stretches out to redshift $z \sim 0.135$ crossing the blazar sightline at $\Delta z = 0.127 - 0.129$.

3. Observations and data reduction

The blazar H 2356-309 has been observed twice with the *Chandra* LETG, as part of two different observational programs. A first 100 ks LETG observation was performed in October 2007 and has been already analyzed in Buote et al. (2009). A second, deeper LETG observation was carried out over the September–December 2008 period, through ten different pointings with exposures ranging from 15 ks to 100 ks, for a total of 496.4ks. The aim of this observation was to secure, with a conservative flux of $1.0 \times 10^{-11} \text{ergs}^{-1} \text{cm}^{-2}$ (0.5-2.0 keV) a 5σ significant detection of an absorber with a column density of at least $9 \times 10^{15} \text{cm}^{-2}$ (this is the 90% lower limit found by Buote et al. 2009) by means of a long 0.5 Ms non-ToO observation. Table 1 shows the log of the observations.

We mention that H 2356-309 has also been observed with XMM for 130 ks and this observation has been analyzed in Buote et al. (2009). We will not use this observation in our analysis since: 1) it adds only 70 counts in 0.06\AA (the XMM-RGS FWHM) which are $\sim 1/4$ the net counts all the *Chandra* data provide in 0.05\AA ; 2) does not reach the wavelengths of the CV transition which, as we will see in §4.2, characterizes the most important intervening system; 3) makes the analysis in §4.2 very complicated due to the presence of several instrumental features very close to the lines we are investigating.

3.1. Chandra reduction

Each *Chandra* observation was reduced with the latest version of the *Chandra Interactive Analysis of Observation* software (CIAO v. 4.1.2, CALDB v. 4.1.2), following the standard processing procedures outlined in the HRC-S/LETG Grating analysis thread², and applying a new (and still not standard) filtering procedure³ on the level 1 event files. This allowed us to greatly reduce the number of background counts, compared to the standard pipeline procedure, while losing only a negligible percentage of source counts, and so greatly increasing the S/N of the background subtracted source spectrum.

²http://asc.harvard.edu/ciao/guides/gspec_hrcsletg.html

³<http://asc.harvard.edu/contrib/letg/GainFilter/>

Table 1: Log of the Chandra observations of H 2356-309.

ObsID	Instrument	Exposure	Date of observation
8120	HRC-S/LETG	96.49	2007-10-11
10497	HRC-S/LETG	53.93	2008-09-19
10498	HRC-S/LETG	77.88	2008-09-22
10499	HRC-S/LETG	58.69	2008-09-29
10500	HRC-S/LETG	16.15	2008-12-25
10577	HRC-S/LETG	81.72	2008-09-17
10761	HRC-S/LETG	42.15	2008-09-27
10762	HRC-S/LETG	35.17	2008-09-25
10764	HRC-S/LETG	100.4	2008-10-10
10840	HRC-S/LETG	15.14	2008-12-23
10841	HRC-S/LETG	15.15	2008-12-28

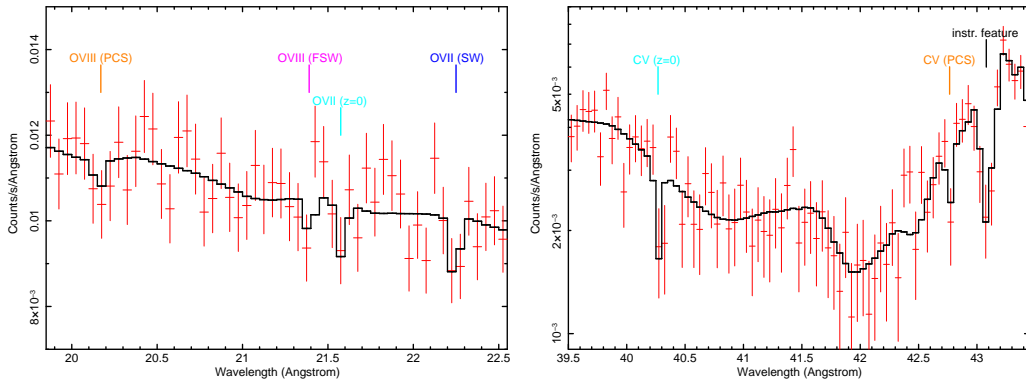


Fig. 2.— Two portions of the spectral regions considered in §4.1. The left panel shows the Chandra spectrum around the rest frame OVII line region while the right panel shows the CV region. Each of the possibly identified lines (modelled in the spectrum with a Gaussian line profile) is labelled with colors indicating different absorbing systems. The fitted redshift of each line is showed in Table 3

For each observation, we produced background light curves and inspected them visually to filter out periods of background flares. Only few observations were affected by short and mild flaring periods and their screening removed a total of just 30 ks, leaving a cleaned total 562 ks exposure.

To maximize the throughput, we used the *Chandra* LETG in combination with the *Chandra* High Resolution Camera for Spectroscopy (HRC-S) dispersion detector. This has virtually no spectral resolution, which prevents the separation of the different spectral orders dispersed by the LETG. We extracted ‘all-order’ negative and positive source and background spectra with the CIAO tool *tg_extract*. Due to impossibility of separating HRC-LETG spectral orders, the spectral modeling of these spectra can only be performed by pre-folding the fitting models with the sum of the convolution products of the redistribution matrices (RMFs) and ancillary responses files (ARFs) belonging to the first N positive and negative orders, respectively. Here N is a number that depends on the intensity of the source, its spectral energy distribution, and the possible presence of strong spectral absorption or emission features, and has to be carefully chosen on an observation by observation base. For our LETG observations of H 2356-309, we verified⁴ that in no case high-energy photons from orders higher than 6 contaminate the low energy spectrum by more than 3% (0.06% at the OVII wavelength). We decided to conservatively build our final “all-order” response matrix by adding up positive and negative orders up to N=10. For each order, we used the ftools task MARFRMF⁵ to ‘multiply’ the RMF by its corresponding ARF. This produced 10 positive and 10 negative normalized RMFs, which we then co-added with the ftools task ADDRMF⁶.

Finally, to maximize the S/N of our spectra, for each observation we co-added negative and positive order source and background spectra (*add_grating_orders* task) and response files (ADDRMF).

Because of our co-adding procedure, particular care must be devoted to account for the wavelength calibration inaccuracy. An updated version of the *degap* polynomial coefficients based on empirical wavelength corrections from multiple HRC-S/LETG observations of Capella has been release since CALDB 3.2⁷. This update allow the correction of the non-linearities in the HRC-S dispersion relation improving the uncertainties across the detector

⁴http://cxc.harvard.edu/ciao/threads/hrcsletg_orders/

⁵<http://heasarc.gsfc.nasa.gov/lheasoft/ftools/caldb/marfrmf.html>

⁶<http://heasarc.gsfc.nasa.gov/lheasoft/ftools/caldb/addrmf.html>

⁷http://cxc.harvard.edu/cal/Letg/Hrc_disp/degap.html

from 0.014\AA to 0.010\AA (RMS deviation). This uncertainty is lower at shorter wavelengths and higher at longer wavelengths. Since we have coadded positive and negative orders we should consider a larger uncertainty. The propagation of the RMS deviations gives an uncertainty of 0.014\AA . However to be conservative we adopt 20m\AA of uncertainty since the updated wavelength corrections have been applied to the rest frame position of the strongest soft X-ray metal electronic transitions and the interpolation of the correction may not be strictly valid to the position of blue- and red-shifted lines.

4. Spectral Analysis

We performed all our spectral analysis with the fitting package *Sherpa* of CIAO (v. 4.1.2). The statistics we used for our fits is the data weighted χ^2 with the Gehrels variance function (Gehrels 1986), the default in *Sherpa*. We first checked for variability of the broad band $10\text{-}50\text{\AA}$ continuum (flux and spectral shape) of H 2356-309, between the 11 *Chandra* observations. We grouped each spectrum at a minimum of 20 counts per bin, and modeled each data-set independently with a power law attenuated by the sightline Galactic column of neutral gas ($N_H = 1.44 \times 10^{20} \text{ cm}^{-2}$; Kalberla et al. 2005). We found that both the source spectral shape and flux varied only moderately (12% and 20%, respectively) between the ten 2008 observations: the $0.3\text{-}1.0$ keV flux ranges within the $1.25 - 1.5 \times 10^{-11} \text{ ergs}^{-1} \text{ cm}^{-2}$ interval, while the power law best fitting spectral indices vary between $\Gamma = 1.96 - 2.20$. The $0.3\text{-}1$ keV source flux during the 2007 observation, is 50-80% lower than during the 2009 observations, but the best fitting power law spectral index of $\Gamma = 2.19 \pm 0.06$ is still in the range measured during the 2008 observations. Since both the $10\text{-}50 \text{ \AA}$ flux and spectral shape of the target varied only moderately between the different observations, and because we are interested in the search of narrow spectral features, which are not affected by broad-band spectral-shape variability, we decided to co-add the HRC-S/LETG spectra of all the observations, to increase the final S/N per resolution element. The resulting spectrum has $\simeq 290$ net source Counts per 50 m\AA Resolution Element (CPRE) and $\sim 120\text{-}160$ background CPRE at 22 \AA , and so a $S/N \sim 11.6 - 12.6$ at 22 \AA . This gives a theoretical $\geq 1\sigma$ sensitivity to absorption lines with $EW \geq 12 - 13 \text{ m\AA}$, at 22 \AA . We grouped the data to half the nominal FWHM of LETG spectra with 25 m\AA per bin for all the subsequent analysis.

4.1. Search for Intervening Absorption Lines

Our main goal is to constrain the warm-hot gaseous content of the two filamentary galaxy structures here identified as PCS and FSW. At the expected WHIM temperatures

Table 2: Strongest Metal Transitions in Gas at $T=10^5 - 10^7$ K

Ion	Wavelength	Oscillator Strength
CV $K\alpha$	40.2678	0.648
CVI $K\alpha$	33.7360	0.416
OVII $K\alpha$	21.6019	0.696
OVIII $K\alpha$	18.9689	0.416
NeIX $K\alpha$	13.4471	0.724
NeX $K\alpha$	12.1339	0.416

the most intense absorption lines are the $K\alpha$ resonant transitions from He- and H-like C, O and Ne. Table 2 lists the rest frame wavelengths and oscillator strengths of these transitions.

A crucial condition for the search for unresolved absorption lines in intrinsically featureless spectra, is the accurate subtraction of the local continuum. A visual inspection of the broad band, 10-50 Å, residuals of the co-added LETG spectrum of H 2356-309, after subtracting the best-fitting absorbed power law, clearly showed the presence of 1-3 Å broad systematics, particularly near or at the wavelength of the main instrumental edges of CI and OI. In general, the residuals deviated significantly from zero, in both directions, in several spectral regions. This makes the assessment of the actual significance of a possible absorption line at such wavelengths, difficult. For each of the two redshifted systems (the PCS and the FSW), we therefore decided to isolate four 3-6 Å broad spectral regions, around the absorption lines of interest (Table 1), at the following rest-frame intervals: 11-14 Å (NeX, NeIX), 18.5-25.0 Å (OVII, OVII), 31.5-34.5 Å (CVI), 39-42 Å (CV). We fitted each of these spectral intervals with continuum models including third-order polynomials. We then inspected visually the residuals to look for possible relatively broad 0.5-1 Å deviations (due to instrumental effects), and, when needed, added to the best-fit polynomial 0.5-1 Å broad emission or absorption Gaussian, to improve the modelling of the local continua. We iterated this procedure until we obtained a satisfactory description of all the local continua, and a visual inspection of the residuals revealed no further deviations.

For each of the transitions listed in Table 2, we then added to the local best-fitting continuum a negative-only Gaussian (i.e. with flux allowed to be only negative in the fit), with wavelength allowed to vary within the redshift intervals of the PCS and the FSW and FWHM frozen to 10 mÅ (unresolved in the LETG), and re-fitted the data. For each line we estimate a single line significance in standard deviations, as the ratio between its best-

fitting flux, and its 1σ error (computed with the *Sherpa* routine *projection*⁸, by leaving both the continua and Gaussian normalizations free to vary). Four and three of the transitions listed in Table 2 were preliminarily, and tentatively, identified at a single line significance $> 1\sigma$, for the PCS (CV, OVII, OVIII, and NeIX) and the FSW (CVI, OVIII and NeIX), respectively. For the remaining transitions we list their 3σ EW upper limits. For comparison, and completeness, Table 3 also lists the result of our fitting procedure for the lines listed in Table 2, at $z \simeq 0$. five of these transitions are detected at $\geq 1\sigma$ at $z \simeq 0$ (CV, OVII, OVIII, NeIX and NeX). What discussed above provides only a preliminary attempt to check for the presence of the expected absorption lines at the redshifts of the Large-Scale galaxy Structures present along the lines of sight. The presence (or absence) of a given line (at the quoted significance level: Table 3) is only used as a guidance for the detailed global fitting procedure presented in next section, and that that makes use of our self-consistent WHIM collisional ionization plus photoionization model.

Figure 2 shows two spectral portions of the total *Chandra* LETG spectrum of H 2356-309, containing the three lines tentatively identified at the redshifts of the PCS and the FSW.

4.2. Constraining the Physics of the Putative PCS and FSW Absorbers with a Self -Consistent WHIM Model

In §4.1 we generally searched for the presence of the strongest absorption metal lines expected from highly ionized gas with temperatures in the broad interval $T = 10^5 - 10^7$ K. However, these transitions belong to ions with quite different ionization potential (e.g CV and NeX) and whose relative abundances critically depend on the ionization mechanisms at work, and on the actual gas temperature. For example, in collisionally ionized gas, OVII, being H-like and so quite stable, is virtually the only abundant ion of O within a broad interval of temperatures, within $\log T(\text{K})=5.5-6.2$. In the same temperature interval the lower ionization ions CV and CVI are relatively abundant, with CV decreasing monotonically from $\sim 75\%$ down to $\sim 5\%$, and CVI raising from $\sim 25\%$ up to $\sim 50\%$ at its $\log T(\text{K})=6$ peak temperature, and then decreasing again down to $\sim 20\%$. On the contrary the higher ionization ions OVIII, NeIX and NeX are only important at the high-temperature extreme of this interval, with relative abundances steeply raising from very low values up to 23% (OVIII), 96% (NeIX) and 3% (NeX). Modeling the spectra of extragalactic sources crossing regions of the Universe with large galaxy overdensities (expected to trace WHIM filaments)

⁸<http://cxc.harvard.edu/sherpa/ahelp/projection.py.html>

with self-consistent ionized absorber models, may therefore provide useful constraints on the ionization state and column density of the putative absorbers embedded in these LSSs, even if the spectral signature of the gas are individually marginally detected (and/or upper limits are obtained) as long as they are modelled jointly.

Here we make use of an adaptation of the Photoionized Absorber Spectral Engine (PHASE; Krongold et al., 2003) code, for WHIM gas (e.g. Nicastro et al. 2009). The code includes more than 3000 electronic resonant transitions (including metal inner-shell) from all elements lighter than Ni, and computes, for a given H equivalent column density, temperature and turbulence velocity of the absorber, the Voigt-profile folded opacity of each transition. The ionization balance in the gas is computed by perturbing the equilibrium collisional ionization balance at a given temperature T , with photoionization by the meta-galactic UV and X-ray background at a given redshift (the redshift of the absorber). Such second-order photoionization contribution depends uniquely on the baryon density n_b in the gas (the lower the density the higher the contribution of photoionization), and it starts to be effective at $n_b \lesssim 10^{-5} \text{ cm}^{-3}$.

In our fitting procedure, we use the same initial methodology adopted in §4.1. For each of the two super-structures, the PCS and the FSW, we fit the 4 different narrow-band portions of the continuum where the main transitions lie, independently. For each spectral interval, our fitting model includes the best-fitting continuum determined in §4.1 attenuated by our hybrid-ionization absorption WHIM model. For each spectral interval we leave free to vary in the fit, the continuum normalization and two out of the five parameters of the WHIM model, namely: the equivalent H column density N_H and the temperature T of the gas. Both N_H and T are linked to their same respective values in the 4 independently fitted spectral regions. The remaining parameters of our WHIM model are the turbulence velocity v (summed in quadrature to the thermal Doppler parameter of a given transition), the redshift z and the baryon density n_b of the absorbers. The baryon density n_b is highly degenerate with the electron temperature (which is set mainly by collisions in shock-heated WHIM gas), and modifies only slightly the ionization balance of the gas, compared with pure collisional equilibrium at a given temperature. Consequently, n_b can be constrained independently of temperature only with data where several transitions from different ions of the same element are clearly detected. In our fit of the putative absorbers at the redshifts of the PCS and the FSW, we therefore freeze the gas baryon density to a typical WHIM value of $n_b = 10^{-5} \text{ cm}^{-3}$. Analogously, the turbulent velocity of the absorber (degenerate with the ion column density for saturated lines), can only be properly constrained when the single absorption lines are resolved and their profile clearly detected at high significance. We freeze this parameter to $v = 100 \text{ km s}^{-1}$, comparable to typical values of Doppler velocities inferred by hydrodynamical simulations (e.g. Cen & Fang 2006). Finally, for each of the

4 spectral regions, we first leave the redshift of the absorbers to vary independently over the entire redshift extent of the two super-structures ($z = 0.060 - 0.063$ for the PCS and $z = 0.127 - 0.129$ for the FSW), and then refine the fitting by freezing the redshift of the absorber in the spectral region where the most significant absorption line is detected to its best fitting value, and leaving the redshifts of the other absorbers in the three remaining spectral regions, free to vary between ± 20 mÅ from the frozen redshift of the most significant absorption line, to account for the 90% systematic wavelength uncertainties in the HRC-S LETG.

Table 4 summarizes the results of our fit. Errors are quoted at a 68% confidence limit. For each parameter listed in table 4, we compute errors by allowing the continuum normalization to vary within its 1σ uncertainty and allowing the other free WHIM model parameters free to vary except in the case of the estimation of $\log N_H$ and $\log T$ errors where we fixed the redshifts to their best-fit value.

4.2.1. The PCS filament

For this structure, we found the possible co-existence of two distinct WHIM phases (Figure 3): a warm phase, traced by CV absorption (Figure 4), with $\log T = 5.35_{-0.13}^{+0.07}$ K and $\log N_H = (19.1 \pm 0.2) \times (Z/Z_\odot)^{-1} \text{ cm}^{-2}$, and a much hotter and less constrained phase, traced by OVIII absorption (Figure 5), with $\log T = 6.9_{-0.8}^{+0.1}$ K and $\log N_H = 20.1_{-1.7}^{+0.3} \times (Z/Z_\odot)^{-1} \text{ cm}^{-2}$.

The redshift interval traced by the distribution of galaxies of the PCS, along the line of sight to H 2356-309, is $0.060 < z < 0.063$. The two WHIM phases tentatively identified here have best-fitting redshifts consistent with each-other, and with the PCS redshift interval, namely: $z_{warm} = 0.0623 \pm 0.0005$ and $z_{hot} = 0.063 \pm 0.001$.

We note that the physical parameters of the putative warm component of the PCS are constrained much better than those of the hot component (Figure 3). This is because the opacity of absorbing gas to light metal transitions decreases with increasing temperatures. At the best-fitting temperature of the hot component of the PCS, only residual opacity from highly ionized O, Ne and Fe is present (Figure 5), and the two free model parameters, temperature and N_H , becomes highly correlated (Figure 3, red, dotted lines), and therefore only poorly constrained. At the temperatures of the warm PCS phase, instead, several strong transitions from a number of abundant ions can still produce enough opacity in the data,

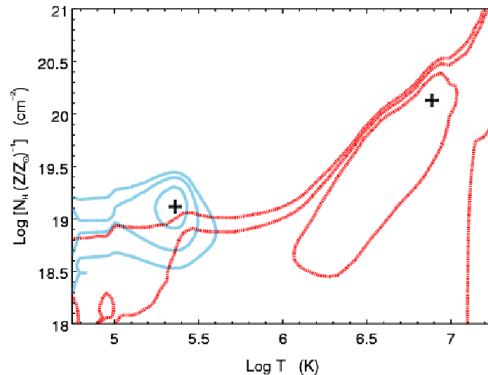


Fig. 3.— 68%, 90% and 95% temperature and equivalent H column density confidence contours for the two putative WHIM phases (warm - solid cyan - and hot - dotted red) permeating the PCS.

which makes T and N_H virtually uncorrelated (Figure 3, cyan solid lines⁹). This can be also seen in Figure 4, where we show two portions of the LETG spectrum of H 2356-309 with the strongest absorption lines from the warm component of the PCS, superimposed to the best-fitting continuum (red line) plus warm WHIM model component (blue line). The right panel of Fig. 4 shows the strongest line of the best-fitting warm-component of the PCS, the CV $K\alpha$ at a redshifted wavelength of $\lambda = 42.776 \text{ \AA}$. However, several other, moderately strong, lines are predicted by this model at shorter wavelengths, and are shown in the left panel of Fig. 4, namely the outer shell OVII $K\alpha$ absorption line at $\lambda = 22.95 \text{ \AA}$ (superimposed on the OI instrumental edge), and the two inner shell $K\alpha$ transitions from OV at $\lambda = 23.74 \text{ \AA}$ ($\lambda = 22.35 \text{ \AA}$ rest frame) and OIV at $\lambda = 24.17 \text{ \AA}$ ($\lambda = 22.75 \text{ \AA}$ rest frame). The data are consistent with the presence of these lines, which tightly constrain the temperature and column density of the warm component of the PCS.

4.2.2. The FSW

For the FSW, the LETG data are consistent with the presence of one hot WHIM component (Figure 3), traced mainly by $K\alpha$ OVIII and NeIX absorption (Figure 7). The best-fitting WHIM parameter of this component are $\log T = 6.6^{+0.1}_{-0.2} \text{ K}$ and $\log N_H = 19.8^{+0.4}_{-0.8} \text{ cm}^{-2}$,

⁹We caution that the opening of the contours at low temperatures is mostly likely a numerical artifact, due to the hitting of the low-temperature end of the model grid, during the error-estimate procedure.

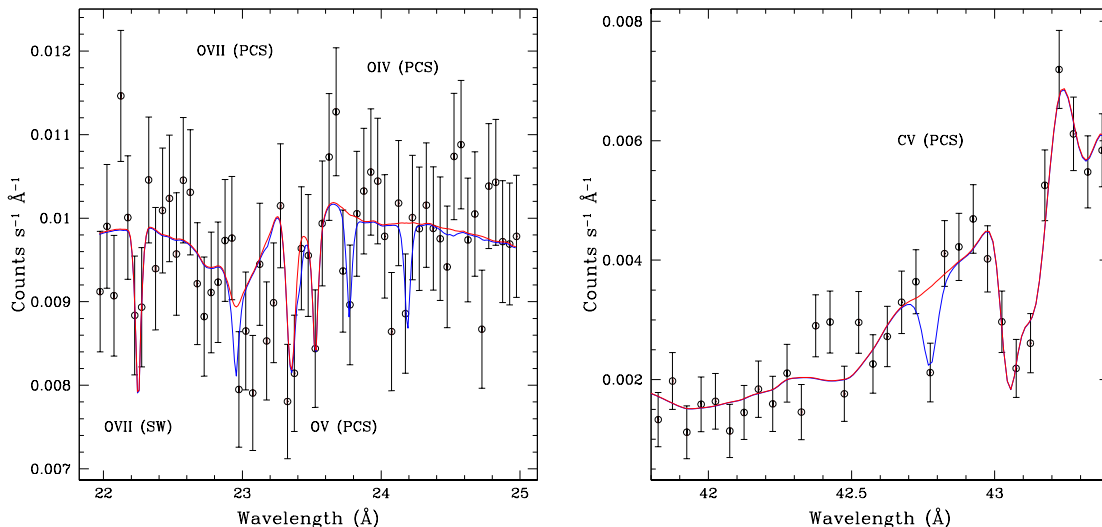


Fig. 4.— Portions of the LETG spectrum of H 2356-309 showing the strongest absorption lines from the warm component of the PCS. The best-fitting continuum model is shown in solid thick red, while absorption lines from the warm WHIM component are shown in solid thin blue. The CV $K\alpha$ absorption line at a redshifted wavelength of $\lambda = 42.776 \text{ \AA}$ is the strongest line of the best-fitting warm-component of the PCS (right panel). The other strong lines predicted by the model are the outer shell OVII $K\alpha$ absorption line at $\lambda = 22.95 \text{ \AA}$ (superimposed on the OI instrumental edge), and the two inner shell $K\alpha$ transitions from OV at $\lambda = 23.74 \text{ \AA}$ ($\lambda = 22.35 \text{ \AA}$ rest frame) and OIV at $\lambda = 24.17 \text{ \AA}$ ($\lambda = 22.75 \text{ \AA}$ rest frame; left panel). Also shown in the left panel are the $z \simeq 0$ OVII $K\alpha$ and the atomic and molecular OI $K\alpha$ lines.

and, as for the hot component of the PCS, they are only poorly constrained, due to the high best-fitting temperature of the gas. The tighter lower limit on the temperature, compared to that of the hot phase of the PCS, is due to the inconsistency of the data with any OVII $K\alpha$ absorption stronger than $EW \geq 5.8 \text{ m\AA}$ (3σ limit; Fig. 7, third panel).¹⁰

The redshift interval traced by the distribution of galaxies of the PCS, along the line of sight to H 2356-309, is $0.127 < z < 0.129$. The WHIM phase tentatively identified here has

¹⁰At the redshift of the putative FSW WHIM component, the OVII $K\alpha$ falls at $\lambda = 24.25 \text{ \AA}$, a region of the detector free of instrumental features, unlike the PCS case, where the OVII $K\alpha$ falls at the exact wavelength of the instrumental OI edge.

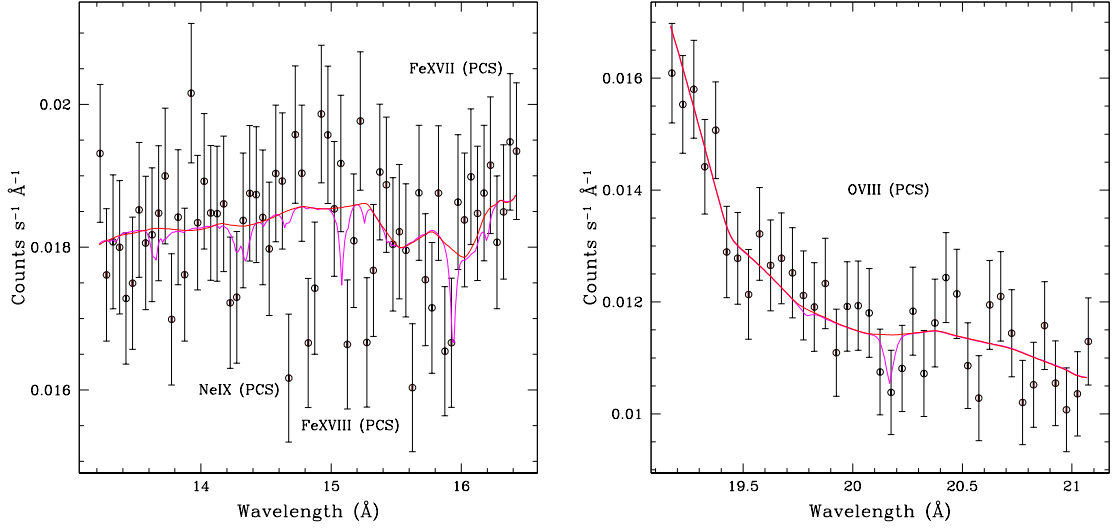


Fig. 5.— Portions of the LETG spectrum of H 2356-309 showing the strongest absorption lines from the hot component of the PCS. The best-fitting continuum model is shown in solid thick red, while absorption lines from the warm WHIM component are shown in solid thin magenta. The OVIII $K\alpha$ absorption line at a redshifted wavelength of $\lambda = 20.17 \text{ \AA}$ is the strongest line of the best-fitting hot-component of the PCS (right panel). The other predicted lines are the NeIX $K\alpha$ absorption line at $\lambda = 14.29 \text{ \AA}$ and two strong L shell transitions from FeXVIII ($\lambda = 15.09 \text{ \AA}$, $\lambda = 14.20 \text{ \AA}$ rest frame) and FeXVII ($\lambda = 15.96 \text{ \AA}$, $\lambda = 15.02 \text{ \AA}$ rest frame; left panel).

best-fitting redshifts consistent at 1σ with the low redshift end of the FSW interval, namely: $z_{FSW-WHIM} = 0.126 \pm 0.001$.

5. Discussion

The line of sight to the blazar H 2356-309 is extremely rich in galaxy large-scale filamentary structures (Figure 1). Other than the SW at least two distinct filaments of galaxies cross this line of sight, at average redshifts $\langle z_1 \rangle = 0.0615$ (the PCS structure) and $\langle z_2 \rangle = 0.128$ (the FSW structure). These very rich structures have line of sight extensions of $D_1 = 12.4$ Mpc and $D_2 = 8$ Mpc, respectively, implying Hubble flow velocity ranges of $\Delta v_1^H = 890 \text{ km s}^{-1}$ and $\Delta v_2^H = 580 \text{ km s}^{-1}$.

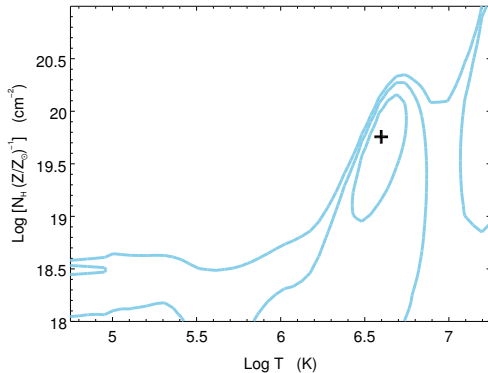


Fig. 6.— 68%, 90% and 95% temperature and equivalent H column density confidence contours for the putative WHIM gas permeating the FSW.

The thermal broadening of C or O lines in gas with $T < 10^7$ K is $b < 85$ km s $^{-1}$ (C) or $b < 74$ km s $^{-1}$ (O), negligible compared to turbulence induced by peculiar motion of the structures. In simulations (e.g. Cen & Ostriker 2006) WHIM intrinsic (i.e. excluding Hubble flow broadening) turbulence are observed to be of ~ 100 km/s. If the PCS and the FSW galaxy structures were homogeneously embedded by WHIM, therefore, the Hubble-flow broadening would be by far the dominant broadening mechanism, and the gas would imprint metal absorption lines with $\text{FWHM} \sim 890$ km s $^{-1}$ and $\text{FWHM} \sim 580$ km s $^{-1}$, for the PCS and the FSW respectively, easily resolved by the HRC-S/LETG ($\text{FWHM} = 750$ km s $^{-1}$ at 20 Å and $\text{FWHM} = 375$ km s $^{-1}$ at 40 Å).

On the contrary, unresolved O absorption lines in the HRC-LETG must imply that the gas is homogeneously spread over a limited portion of these two galaxy structures, extending not more than 4 Mpc along the line of sight (corresponding to Hubble-flow broadening of 0.021 Å at 20 Å, i.e. 1σ of the LETG Line Spread Function)

5.1. On the OVII Bearing WHIM or Galaxy Halo Gas

Our total *Chandra* LETG spectrum of H 2356-309 is sensitive to absorption line $\text{EW} \geq 14$ mÅ at 22 Å, at $\geq 3\sigma$ confidence level. For unsaturated lines ($b \gtrsim 200$ km s $^{-1}$) this corresponds to OVII column densities $N_{\text{OVII}} \geq 3.4 \times 10^{15} (1+z)^{-1}$ cm $^{-2}$. At overdensities $\delta \simeq 50(1+z)^{-3}$ and temperature $T \simeq 10^6$ K, typical of the bulk ($\sim 50\%$) of the WHIM density-temperature distribution (e.g. Cen & Ostriker 2006), and assuming homogeneity, these columns correspond to line of sight extensions of the filament of $D \geq$

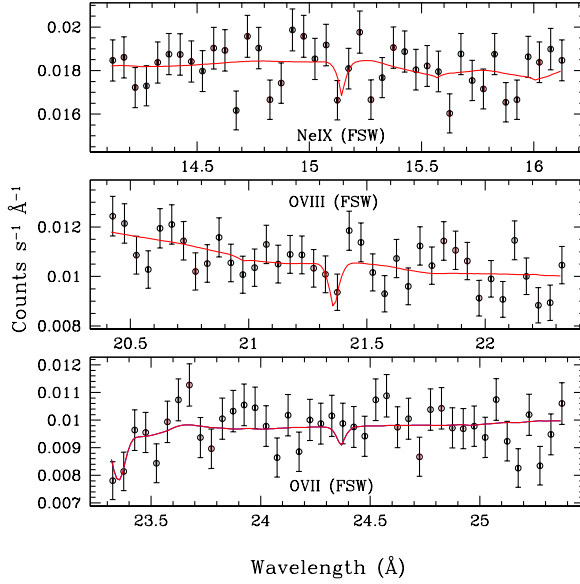


Fig. 7.— Portions of the LETG spectrum of H 2356-309 where the strongest absorption lines from the putative WHIM component of the FSW lie. The OVIII $K\alpha$ absorption line at a redshifted wavelength of $\lambda = 21.36 \text{ \AA}$ is the strongest line of the best-fitting FSW WHIM model (central panel). The other moderately strong predicted line is the NeIX $K\alpha$ absorption line at $\lambda = 15.14 \text{ \AA}$ (top panel). In the third panel we also show the region where the OVII $K\alpha$ absorption line of the best-fitting FSW WHIM model falls: the data are clearly incompatible with the presence of such a line.

$N_b/n_b = [[N_{OVII}/(A_O f_{OVII})]/n_b](Z/Z_\odot)^{-1} \simeq 1.4(Z/Z_{0.1\odot})^{-1} \text{ Mpc}$ (where we assumed $A_O = 8.5 \times 10^{-4}$, Grevesse & Anders 1989, and a relative fraction of OVII $f_{OVII} = 0.9$). The extensions of the PCS and FSW galaxy structures, if entirely permeated by WHIM gas representative of the bulk of its density-temperature distribution, should then guarantee the high-significance detection of strong OVII absorbers. This has proven to be true only for the SW (Fang et al. 2009) which is the most extended structure along the line of sight with $D = 16.6 \text{ Mpc}$.

We did not detect strong (i.e. $N_{OVII} \geq 3.4 \times 10^{15}(1+z)^{-1} \text{ cm}^{-2}$ at $\geq 3\sigma$), unresolved (i.e. $b \leq 285 \text{ km s}^{-1}$ at 1σ) OVII absorption along either of the other two LSSs crossing the line of sight to H 2356-309, the PCS and the FSW. These non-detections tell us that any ionized gas at typical WHIM temperatures ($T \sim 10^6 \text{ K}$) embedded in the 4 Mpc cores (i.e. imprinting unresolved O lines: see §5) of the line of sight extent of the PCS and the FSW structures must have overdensities $\delta \leq 18(Z/Z_{0.1\odot})^{-1}(1+z)^{-4}$ (where the additional

$(1+z)^{-3}$ term comes from the $(1+z)^3$ redshift dependency of $\langle n_b \rangle$. For both the PCS ($\delta \leq 14(Z/Z_{0.1\odot})^{-1}$ at $\geq 3\sigma$), and the FSW ($\delta \leq 11(Z/Z_{0.1\odot})^{-1}$ at $\geq 3\sigma$) these overdensities lie on the lower end of the predicted overdensity interval for the bulk of the WHIM, ranging between $\delta \simeq 5 - 50$. This is the opposite of what intuitively expected (though with a large scatter, e.g. Viel et al., 2005), that richer galaxy LSSs potentially harbor denser WHIM filaments.

Alternatively the OVII bearing gas in these structures, could spread over the large extent of the galaxy super-structure along the line of sight, and so produce broader and resolved shallow (hence more difficult to detect) lines in the LETG (see §5), or could have metallicity lower than 10% Solar, in either cases relaxing the above limits on the gas overdensities. However, any denser WHIM gas at the typical $T \sim 10^6$ K temperature and with line of sight turbulence velocity lower than a few hundreds km s^{-1} , should have been detected at high significance in the LETG spectrum of H 2356-309.

An alternative interpretation of the OVII absorption, is that it could be associated with the hot extended halo of a single galaxy with small line of sight impact parameter. In this scenario, if r is the galaxy spherical halo radius, the impact parameter d must be smaller than r , and the line of sight can only cross a section of the halo $D = 2r \sin(\alpha)$, where $0 \leq \alpha \leq \pi/2$ is the angle between the direction of the galaxy-line of sight impact parameter d and the halo radius r in the direction of the interception of the halo external boundary with the line of sight. By averaging over $0 \leq \alpha \leq \pi/2$, we get $\langle D \rangle = 4r/\pi$. With this assumptions the baryon density of the galaxy halo is given by $n_b = N_b/D \lesssim [N_{OVII}/(A_{OVII})]/(4d/\pi)(Z/Z_{\odot})^{-1}$.

The non-detection of OVII bearing gas up to the $N_{OVII} \geq 3.4 \times 10^{15} (1+z)^{-1} \text{ cm}^{-2} 3\sigma$ limit, allows us to estimate stringent upper limits on the densities of putative galaxy halo gas with $T \sim 10^6$ K intercepting the line of sight to H 2356-309 at the redshifts of the PCS and the FSW structures. By using an impact parameters $200 \lesssim d \lesssim 300$ kpc (Stocke et al. 2006), we obtain $n_b \simeq (3 - 5) \times 10^{-5} (Z/Z_{0.1\odot})^{-1} \text{ cm}^{-3}$ for both the PCS and the FSW which is lower than the values derived for our galaxy halo or extended Local Group gas (e.g. Rasmussen et al. 2003; Williams et al. 2005). These values would be raised at most by a factor of 2 by accounting for non constant gas density profile¹¹.

¹¹We assumed a β – model (Cavaliere & Fusco-Femiano 1976) gas density distribution with β parameter ranging between 0.6 and 0.9 and assumed core radius ranging from 1 kpc to an unrealistically high 400 kpc value.

5.2. The Ionized Gas Content of the PCS and FSW Galaxy Structures

As discussed in the previous section, we do not detect significant amount of OVII-bearing (i.e. typical of the bulk WHIM temperature-density distribution) gas in either the PCS or the FSW galaxy super-structures. However, at the redshift of these structure, we do marginally detect a number of (individually low-significance) metal absorption lines, from either low-ionization (OVI, OV, CV) or high-ionization (OVIII, NeIX) ions. Such ions populate gas with temperatures in the low- or high-end of the WHIM temperature distribution, containing roughly 27% and 23% of the predicted WHIM mass, respectively. The absorption lines hinted in the LETG spectrum of H 2356-309 at the redshifts of the PCS and the FSW, are all unresolved, which implies line of sight extensions of the absorber $D \lesssim 4$ Mpc.

Despite the low statistical significance of each of these individual absorption lines, we were still able to constrain the main physical parameters of the absorbing gas, namely its equivalent H column density and temperature, by modelling the broad-band LETG data with our hybridly ionized WHIM gas model. We identify two different absorbing WHIM phases at the redshift of the PCS, with $\log T = 5.35_{-0.13}^{+0.07}$, $\log N_{\text{H}} = 19.1 \pm 0.2(Z/Z_{\odot})^{-1}$, and $\log T = 6.9_{-0.8}^{+0.1}$, $\log N_{\text{H}} = 20.1_{-1.7}^{+0.3}(Z/Z_{\odot})^{-1}$, for the warm and the hot phases respectively. For the FSW, instead, only one hot phase is tentatively detected, with $\log T = 6.6_{-0.2}^{+0.1}$ and $\log N_{\text{H}} = 19.8_{-0.8}^{+0.4}(Z/Z_{\odot})^{-1}$.

We can infer baryon densities lower limits for these systems, by assuming that the absorbers are embedded in their galaxy superstructures, and have dense cores extending < 4 Mpc along the line of sight (we note that for the two phases in the PCS, assuming their are physically separated, the total extent can be close to the entire line of sight extension of the PCS galaxy filament). By conservatively assuming the -1σ N_{H} value as N_{b} for the two PCS WHIM phases we get $n_{\text{b}}(\text{Warm}) = N_{\text{b}}(\text{Warm})/D > 6.4 \times 10^{-7}(Z/Z_{\odot})^{-1} \text{ cm}^{-3}$ ($\delta > 2.7(Z/Z_{\odot})^{-1}$) and $n_{\text{b}}(\text{hot}) = N_{\text{b}}(\text{hot})/D > 2.0 \times 10^{-7}(Z/Z_{\odot})^{-1}$ ($\delta > 0.9(Z/Z_{\odot})^{-1}$), while for the hot phase of the FSW we obtain $n_{\text{b}} = N_{\text{b}}/D > 8.1 \times 10^{-7}(Z/Z_{\odot})^{-1}$ ($\delta > 2.8(Z/Z_{\odot})^{-1}$), all consistent with predicted WHIM overdensities.

5.3. Number density of OVII absorbers along the line of sight to H 2356-309

From our best-fitting WHIM model temperatures for the three putative WHIM absorbers at the redshifts of the PCS and the FSW, we can infer the relative fraction of OVII in each phase. These are $f_{\text{OVII}}^{W-PCS} = 0.15$, $f_{\text{OVII}}^{H-PCS} = 9 \times 10^{-4}$ and $f_{\text{OVII}}^{FSW} = 0.028$. These ion fractions correspond to columns of $N_{\text{OVII}}^{W-PCS} = 1.6_{-0.6}^{+1.8} \times 10^{15} \text{ cm}^{-2}$, $N_{\text{OVII}}^{H-PCS} = 9.6_{-9.4}^{+9.5} \times 10^{13}$

cm^{-2} and $N_{OVII}^{FSW} = 1.5_{-1.3}^{+2.3} \times 10^{15} \text{ cm}^{-2}$, or to unsaturated OVII EWs of $7_{-3}^{+8} \text{ m}\text{\AA}$, $0.42_{-0.41}^{+0.42} \text{ m}\text{\AA}$ and $7_{-6}^{+11} \text{ m}\text{\AA}$, respectively.

Assuming the best-fitting temperature and N_H values as face values, the lowest OVII equivalent width that we are indirectly probing, through our hybrid-ionization WHIM code, along the line of sight to H 2356-309, is therefore $\text{EW}(\text{OVII}) \gtrsim 0.4 \text{ m}\text{\AA}$, corresponding to the hot phase of the PCS. Combining our three tentative WHIM detections, with the WHIM detection associated with the SW, leaves us with 4 distinct WHIM systems with $\text{EW}(\text{OVII}) \geq 0.4 \text{ m}\text{\AA}$, along a $\Delta z = 0.165$ path length, or a number density of $\text{EW}(\text{OVII}) \geq 0.4 \text{ m}\text{\AA}$ filaments of $dN(\text{EW} > 0.4)/dz = 24.2_{-11.6}^{+19.2}$ (allowing for the large 1σ uncertainties due to the small number statistics, i.e. Gehrels 1986). This is fully consistent with hydrodynamical simulation predictions (e.g. Cen & Fang 2006).

We can, in principle, also compute the cumulative number density of OVII filaments per unit redshifts, with EW larger than a given threshold, for two additional EW thresholds: $\geq 7 \text{ m}\text{\AA}$ (3 absorbers) and $\geq 25.8 \text{ m}\text{\AA}$ (1 absorber: Fang et al. 2009). We get $dN(\text{EW} > 7)/dz = 18.2_{-9.9}^{+17.7}$ and $dN(\text{EW} > 25.8)/dz = 6.1_{-5.1}^{+13.9}$. We plot such derived number density per unit redshift, in Figure 8, superimposed to the theoretical cumulative $dN(> \text{EW}_{\text{thresh}})/dz$ curve from Cen & Fang (2006). The data-point at $25.8 \text{ m}\text{\AA}$, exceeds the predictions by more than 2σ . This could be due to a line of sight selection bias, or may reflect the possibility that one or more of the detected absorption do not actually arise in tenuous WHIM filaments, but in much denser galaxy halos of one (or more) components of the LSSs with line of sight impact parameter of $\sim 200 - 300 \text{ kpc}$. It may finally be that the most marginally detected systems, the Hot-PCS and the FSW, given their large uncertainties in temperature and column density may just be explained as occasional statistical fluctuation. In this case, considering only the SW and Warm-PCS systems, the number density of $\text{EW}(\text{OVII}) \geq 7 \text{ m}\text{\AA}$ filaments would be $dN(\text{EW} > 7)/dz = 12.1_{-11.7}^{+16.0}$ which within the large uncertainties is consistent with the predictions (see Figure 8 dashed data point).

5.4. Cosmological Mass Density of the WHIM from the H 2356-309 Line of Sight Absorbers

Finally, we derive the Cosmological mass density of the WHIM as measured along the line of sight to H 2356-309, by assuming that all 4 different phases seen at the redshifts of the three SW, PCS and FSW galaxy superstructures are intervening WHIM filaments. By propagating in quadrature the large errors associated with the equivalent H column density measurements of the absorbers, and those intrinsic with cosmic variance low-number statistics, we obtain: $\Omega_b^{WHIM} = (0.021_{-0.018}^{+0.031})(Z/Z_\odot)^{-1}$. This is consistent with the cos-

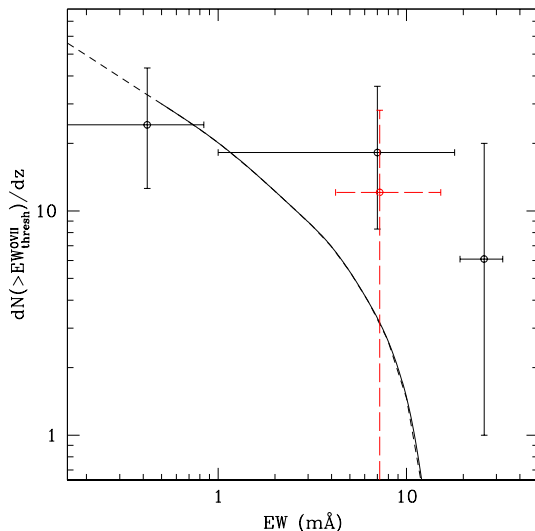


Fig. 8.— Cumulative number density of OVII absorbers per unit redshifts compared to the predictions by Cen & Fang (2006). The dashed line is an extrapolation of the theoretical curve. The dashed data point is obtained by excluding the two most marginally detected systems: the hot-PCS and FSW.

mological mass density of intergalactic Missing Baryons ($\Omega_b^{missing-IGM} \simeq 0.016 \pm 0.005$, e.g. Fukugita & Peebles 2004) in the local Universe, but assumes solar metallicities. Metallicities of $\lesssim 10\%$ Solar, would give an Ω_b^{WHIM} in excess by $\geq 1\sigma$ compared to $\Omega_b^{missing-IGM}$, again probably indicating an intrinsic line of sight selection bias, or simply reflecting the possibility that one or more of the detected absorptions are not imprinted by tenuous WHIM filaments. Again as in previous section we excluded from the analysis the most uncertain systems Hot-PCS and FSW and estimated an $\Omega_b^{WHIM} = (0.0026_{-0.0018}^{+0.0058})(Z/Z_\odot)^{-1}$ which is consistent with the predicted missing baryons by assuming 10% solar metallicity.

6. Conclusions

We have analyzed a long integration (600 ksec) Chandra HRC-S/LETG spectrum of the blazar H 2356-309 to search and characterize the WHIM in two large-scale galaxy structures along this line of sight and, more specifically, the “Pisces-Cetus Supercluster” (PCS) at $z=0.062$ and the “Farther Sculptor Wall” (FSW) at $z=0.128$. These are structures more prominent and more distant with respect to the “Sculptor Wall”, at $z=0.03$, where WHIM was identified in previous works through the detection of the OVII absorption line.

Although we do not detect significant individual absorption lines in the PCS nor in the FSW, the joint analysis of the marginally detected lines (as well as of stringent upper limits) through a self-consistent hybrid ionization spectral model, allow us to constrain the physics of the WHIM in the two farther superstructures. The main results are summarized in the following:

- At the redshift of the PCS we identify two distinct phases: a warm phase, with $\log T = 5.35_{0.13}^{+0.07}$ K and $\log N_{\text{H}} = (19.1 \pm 0.2)$ cm^2 , and a much hotter less significant phase, with $\log T = 6.9_{0.8}^{+0.1}$ K and $\log N_{\text{H}} = 20.1_{-1.7}^{+0.3}$ cm^{-2} (1σ errors).
- At the redshift of the FSW only one hot component is hinted in the data, with $\log T = 6.6_{0.2}^{+0.1}$ K and $\log N_{\text{H}} = 19.8_{-0.8}^{+0.4}$ cm^{-2} .
- Under the assumption that the absorbers are embedded in their galaxy superstructures having baryonic column densities N_b equal to the -1σ N_H value, and have dense cores extending <4 Mpc along the line of sight, we can infer conservative lower limits on the baryons densities in the two systems for the three absorbers. More specifically, for the two PCS WHIM phases we get $\delta > 2.7(Z/Z_{\odot})^{-1}$ and $\delta > 0.9(Z/Z_{\odot})^{-1}$, while for the hot FSW phase we obtain $\delta > 2.8(Z/Z_{\odot})^{-1}$, all consistent with predicted WHIM overdensities.
- By combining the constraints on the OVII absorbers in the PCS and in the FSW, with the previous detection in the SW (Fang et al. 2009), we derive the cumulative number density of OVII absorbers per unit redshift, as a function of the EW(OVII). While at low equivalent widths ($\text{EW(OVII)} > 0.4$ mÅ) the absorbers number density is fully consistent with the predictions of hydrodynamical simulations, at $\text{EW(OVII)} > 10$ mÅ the inferred absorbers number density exceeds significantly the theoretical predictions. The latter finding may result from a line of sight selection bias, or may reflect the possibility that one or more of the detected absorptions do not arise in WHIM filaments but in galaxy halos. We considered also the possibility that the two most marginally detected systems (Hot-PCS and FSW) may be just statistical fluctuations and not absorbers. In this case the number density of OVII absorbers per unit redshift would agree with the predictions within the large uncertainties.
- Finally, by combining the measurements in all absorbers we derive a cosmological mass density of the WHIM of $\Omega_{\text{b}}^{\text{WHIM}} = (0.021_{-0.018}^{+0.031})(Z/Z_{\odot})^{-1}$, consistent with the cosmological mass density of intergalactic missing baryons in the local universe. Yet, if the WHIM metallicities are $<10\%$ Solar, then the resulting $\Omega_{\text{b}}^{\text{WHIM}}$ is significantly in excess of the missing baryon density, again possibly indicating a line of sight selection

bias, or reflecting the possibility that one or more absorbers are not associated with WHIM. The exclusion of the two most marginally detected systems may bring in agreement the Ω_b^{WHIM} value if we assume $0.1Z_\odot$.

We thank the anonymous referee for comments and suggestions which improved the paper presentation. We thank Jeremy Drake for useful discussion and support on Chandra LETG calibration. We also thank Yair Krongold for providing the latest version of his hybrid-ionization WHIM models, and Doug Burke for writing the interface routines between Sherpa and our hybrid-ionization models. FN and LZ acknowledge support from the LTSA grant NNG04GD49G and the ASI-AAE grant I/088/06/0. FN acknowledges support from the FP7-REGPOT-2007-1 EU grant No. 206469. This research has made use of the NASA/IPAC Extragalactic Database (NED) which is operated by the Jet Propulsion Laboratory, California Institute of Technology, under contract with the National Aeronautics and Space Administration.

REFERENCES

- Buote, D. A., Zappacosta, L., Fang, T., Humphrey, P. J., Gastaldello, F., & Tagliaferri, G. 2009, *ApJ*, 695, 1351
- Burns, J. O. & Batuski, D. J. 1984, in *ASSL Vol. 111: Clusters and Groups of Galaxies*, 43–+
- Cavaliere, A. & Fusco-Femiano, R. 1976, *A&A*, 49, 137
- Cen, R. & Fang, T. 2006, *ApJ*, 650, 573
- Cen, R., Kang, H., Ostriker, J. P., & Ryu, D. 1995, *ApJ*, 451, 436
- Cen, R. & Ostriker, J. P. 1999, *ApJ*, 514, 1
- . 2006, *ApJ*, 650, 560
- Colless, M., Peterson, B. A., Jackson, C., Peacock, J. A., et al. 2003, *ArXiv Astrophysics e-prints*
- da Costa, L. N., Pellegrini, P. S., Sargent, W. L. W., Tonry, J., Davis, M., Meiksin, A., Latham, D. W., Menzies, J. W., & Coulson, I. A. 1988, *ApJ*, 327, 544
- Davé, R., Cen, R., Ostriker, J. P., Bryan, G. L., Hernquist, L., et al. 2001, *ApJ*, 552, 473

- Fang, T., Buote, D. A., Humphrey, P. J., Canizares, C. R., Zappacosta, L., Maiolino, R., Tagliaferri, G., & Gastaldello, F. 2009, ArXiv e-prints
- Fukugita, M., Hogan, C. J., & Peebles, P. J. E. 1998, *ApJ*, 503, 518
- Fukugita, M. & Peebles, P. J. E. 2004, *ApJ*, 616, 643
- Gehrels, N. 1986, *ApJ*, 303, 336
- Grevesse, N. & Anders, E. 1989, in *American Institute of Physics Conference Series*, Vol. 183, *Cosmic Abundances of Matter*, ed. C. J. Waddington, 1–8
- Hellsten, U. et al. 1998, *ApJ*, 509, 56
- Jones, D. H., Saunders, W., Colless, M., Read, M. A., Parker, Q. A., et al. 2004, *MNRAS*, 355, 747
- Kaastra, J. S., Lieu, R., Tamura, T., Paerels, F. B. S., & den Herder, J. W. 2003, *A&A*, 397, 445
- Kalberla, P. M. W., Burton, W. B., Hartmann, D., Arnal, E. M., Bajaja, E., Morras, R., & Pöppel, W. G. L. 2005, *A&A*, 440, 775
- Nicastro, F., Krongold, Y., Fields, D., Conciatore, M. L., Zappacosta, L., Elvis, M., Mathur, S., & Papadakis, I. 2009, ArXiv e-prints
- Nicastro, F., Mathur, S., & Elvis, M. 2008, *Science*, 319, 55
- Nicastro, F., Mathur, S., Elvis, M., Drake, J., Fiore, F., Fang, T., Fruscione, A., Krongold, Y., Marshall, H., & Williams, R. 2005a, *ApJ*, 629, 700
- Nicastro, F. et al. 2005b, *Nature*, 433, 495
- Perna, R. & Loeb, A. 1998, *ApJ*, 503, L135+
- Porter, S. C. & Raychaudhury, S. 2005, *MNRAS*, 364, 1387
- Rasmussen, A., Kahn, S. M., & Paerels, F. 2003, in *astro-ph/0301183*, 109–+
- Rasmussen, A. P. et al. 2007, *ApJ*, 656, 129
- Scharf, C., Donahue, M., et al. 2000, *ApJ*, 528, L73
- Stocke, J. T., Penton, S. V., Danforth, C. W., Shull, J. M., Tumlinson, J., & McLin, K. M. 2006, *ApJ*, 641, 217

- Tully, R. B., Scaramella, R., Vettolani, G., & Zamorani, G. 1992, *ApJ*, 388, 9
- Viel, M., Branchini, E., Cen, R., Ostriker, J. P., Matarrese, S., Mazzotta, P., & Tully, B. 2005, *MNRAS*, 360, 1110
- Werner, N., Finoguenov, A., Kaastra, J. S., Simionescu, A., Dietrich, J. P., Vink, J., & Böhringer, H. 2008, *A&A*, 482, L29
- Williams, R. J., Mathur, S., Nicastro, F., Elvis, M., Drake, J. J., Fang, T., Fiore, F., Krongold, Y., Wang, Q. D., & Yao, Y. 2005, *ApJ*, 631, 856
- Zappacosta, L. 2005, in *Chandra Proposal*, 2041–+
- Zappacosta, L. 2006, in *XMM-Newton Proposal ID #05043713*, 165–+
- Zappacosta, L. et al. 2002, *A&A*, 394, 7
- . 2005, *MNRAS*, 357, 929

Table 3: Best-Fitting Absorption Line Parameters and Ids for the PCS and the FSW

Wavelength (in Å)	EW (in mÅ)	Significance ^a (in σ)	Identification	Redshift ^b
Pisces-Cetus Supercluster (PCS)				
42.770 ± 0.015	19.6 ± 13.1	1.5	CV $K\alpha$	0.0621 ± 0.0004
35.76 – 35.86	< 5.5	NA	CVI $K\alpha$	0.060 – 0.063
22.970 ± 0.015	6.2 ± 5.5	1.1	OVII $K\alpha$	0.0633 ± 0.0008
20.160 ± 0.015	7.3 ± 4.8	1.5	OVIII $K\alpha$	0.0628 ± 0.0007
14.280 ± 0.015	5.0 ± 3.3	1.5	NeIX $K\alpha$	0.062 ± 0.001
12.86 – 12.90	< 3.2	NA	NeX $K\alpha$	0.060 – 0.063
Farther Sculptor Wall (FSW)				
45.38 – 45.46	< 6.1	NA	CV $K\alpha$	0.127 – 0.129
38.042 ± 0.015	10.4 ± 8.5	1.2	CVI $K\alpha$	0.1278 ± 0.0004
24.32 – 24.39	< 5.8	NA	OVII $K\alpha$	0.126 – 0.129
21.396 ± 0.015	7.7 ± 4.9	1.6	OVIII $K\alpha$	0.1279 ± 0.0008
15.161 ± 0.015	4.0 ± 3.3	1.2	NeIX $K\alpha$	0.127 ± 0.001
12.46 – 12.47	< 3.1	NA	NeX $K\alpha$	0.127 – 0.129
$z \simeq 0$				
40.274 ± 0.015	38.5 ± 12.3	3.1	CV $K\alpha$	0.0002 ± 0.0005
33.72 – 33.75	< 7.1	NA	CVI $K\alpha$	± 0.0004
21.561 ± 0.015	8.1 ± 5.0	1.6	OVII $K\alpha$	-0.0019 ± 0.0007
18.952 ± 0.015	4.6 ± 3.6	1.3	OVIII $K\alpha$	-0.0009 ± 0.0008
13.449 ± 0.015	7.6 ± 3.3	2.3	NeIX $K\alpha$	± 0.001
12.131 ± 0.015	7.7 ± 2.9	2.7	NeX $K\alpha$	± 0.001

^a Single Line Significance in Standard Deviations, evaluated as the ratio between the best fitting EW and its 1σ error (see text for details).

^b The error is derived from the systematic 1σ wavelength uncertainty of ± 15 mÅ due to the non-linearity of the HRC-S LETG dispersion relationship.

Table 4: Redshift and physical parameters resulting from the fits

$\log T$ (in K)	$\log N_H$ (in $(Z/Z_\odot)^{-1} \text{ cm}^{-2}$)	Redshift
PCS (z=0.06-0.063: Warm Phase)		
$5.35^{+0.07}_{-0.13}$	19.1 ± 0.2	0.0623 ± 0.0005
PCS (z=0.06-0.063: Hot Phase)		
$6.9^{+0.1}_{-0.8}$	$20.1^{+0.3}_{-1.7}$	0.063 ± 0.001
FSW (z=0.127-0.129)		
$6.6^{+0.1}_{-0.2}$	$19.8^{+0.4}_{-0.8}$	0.126 ± 0.001